Available online at www.sciencedirect.com
SCIENCE DIRECT®
Nuclear Instruments and Methods in Physics Research A 555 (2005) 435–450
NUCLEAR INSTRUMENTS & METHODS IN PHYSICS RESEARCH Section A
www.elsevier.com/locate/nima

Technical note

The precision tracker of the OPERA detector

R. Zimmermann[a,*], J. Ebert[a,1], C. Hagner[a], B. Koppitz[a], V. Saveliev[b], W. Schmidt-Parzefall[a], J. Sewing[a], Y. Zaitsev[c]

[a]*Institut für Experimentalphysik, Universität Hamburg, D-22761 Hamburg, Germany*
[b]*Obninsk State University OSU, 249030 Obninsk, Russia*
[c]*ITEP Moscow, 117259 Moscow, Russia*

Received 21 June 2005; received in revised form 22 August 2005; accepted 5 September 2005
Available online 6 October 2005

Abstract

The Precision Tracker of the muon spectrometer of the OPERA detector consists of ~10000 aluminum drift tubes of 8 m length. They have an outer diameter of 38 mm and a wall thickness of 0.85 mm. The challenge of the detector design originates from the 8 m length of the drift tubes, a detector length, which has not been used before. Tight mechanical tolerances for positioning and alignment of the signal wires are required in order to make a significant measurement of the sign of the muon charge.

The detector is manufactured in modules, which are 50 cm wide, each consisting of four adjacent drift tube planes. This guarantees high efficiency and complete rejection of the left–right ambiguity. The details of the novel mechanical design are described in this paper.

For safety reasons, the drift tubes are operated with an Argon/CO_2 gas mixture. The gas volume of the drift tubes is entirely sealed with O-rings, in order to avoid ageing problems. The total gas volume amounts to about 80 m^3.

The front end electronics of the drift tubes consist of a bootstrap amplifier followed by a commercial ultrafast comparator. Thus only digital LVDS signals are transmitted over large distances.

We report on the development and performance of the first two prototype modules of the precision tracker including test measurements of the resolution and efficiency obtained.

PACS: 14.60.Pq; 29.40.Cs; 29.40.Gx; 95.55.Vj

Keywords: OPERA; Neutrino; Drift tube; Attenuation; Efficiency; Gas detector; Tension

1. Introduction

OPERA consists of two massive lead-emulsion target sections followed by muon spectrometers, designed for a long-baseline neutrino oscillation experiment [1]. OPERA will search for ν_τ appearance originating from $\nu_\mu \longleftrightarrow \nu_\tau$ oscillations in the parameter region indicated by the atmospheric neutrino experiments. It exploits nuclear emulsions for the unambiguous detection of the decay of the τ produced in ν_τ CC interactions. This technique was successfully applied in Donut [2] and CHORUS [3]. OPERA will run at the LNGS[2] in the future CNGS[3] neutrino beam from CERN [4]. The detector target mass of ~1.8 kt is needed to reach the required sensitivity to measure $11\nu_\tau$ events in five years for $\Delta m^2 = 2.4 \times 10^{-3}$ eV^2 and 4.5×10^{19} protons on target (pot) per year [5].

The spectrometers will be used for muon identification, the determination of the muon momentum and sign of the muon charge. The task of the muon spectrometer is to clarify the signature of the muonic τ decay and to remove the background originating from charmed particles produced in μ-neutrino interactions.

*Corresponding author. Tel.: +49 40 89984872; fax: +49 40 89982101.
E-mail address: raoul.zimmermann@desy.de (R. Zimmermann).

[1]Supported by the Bundesministerium für Bildung und Forschung, under contract number 05 GH1GUA/9.

[2]Laboratori Nazionali del Gran Sasso.
[3]CERN Neutrinos to Gran Sasso.

0168-9002/$ - see front matter © 2005 Elsevier B.V. All rights reserved.
doi:10.1016/j.nima.2005.09.003

The muon spectrometers shown in Fig. 1 use warm iron core dipole magnets. Each magnet consists of two vertical walls of rectangular cross section having on top and bottom flux return paths surrounded by coils. The magnet walls are made of iron plates of 5 cm thickness interleaved with RPCs, which measure the range of the muons.

This novel muon spectrometer design has the advantage, that only one track coordinate has to be measured precisely, whereas for the commonly used toroidal muon spectrometers space points must be measured.

The precision tracker (PT) measures the muon track coordinates in the horizontal plane. It is made of drift tubes which are located in front and behind the magnet as well as between the two magnet walls (Fig. 1). The PT consists of 12 drift tube planes, each covering an area of $8\,\mathrm{m} \times 8\,\mathrm{m}$.

The present note describes the mechanical design of the Precision Tracker, its readout electronics and the test results of the first prototypes.

2. The specification of the precision tracker

2.1. Resolution

The structure of the muon spectrometer is defined by the task to measure the sign of the muon charge with a significance of at least 4σ. This means, that the momentum resolution of the spectrometer must be better than

$$\frac{\Delta p}{p} \leqslant 0.25 \tag{1}$$

for all muon momenta p up to a maximum of $p = 25\,\mathrm{GeV}/c$.

A muon traversing the spectrometer magnets is deflected twice by an angle $\theta/2$, forming an S-shaped track. The total deflection angle θ is the sum of the amounts of the two deflections. If the positions of the drift tube planes are chosen as shown in Fig. 2 the deflection angle θ

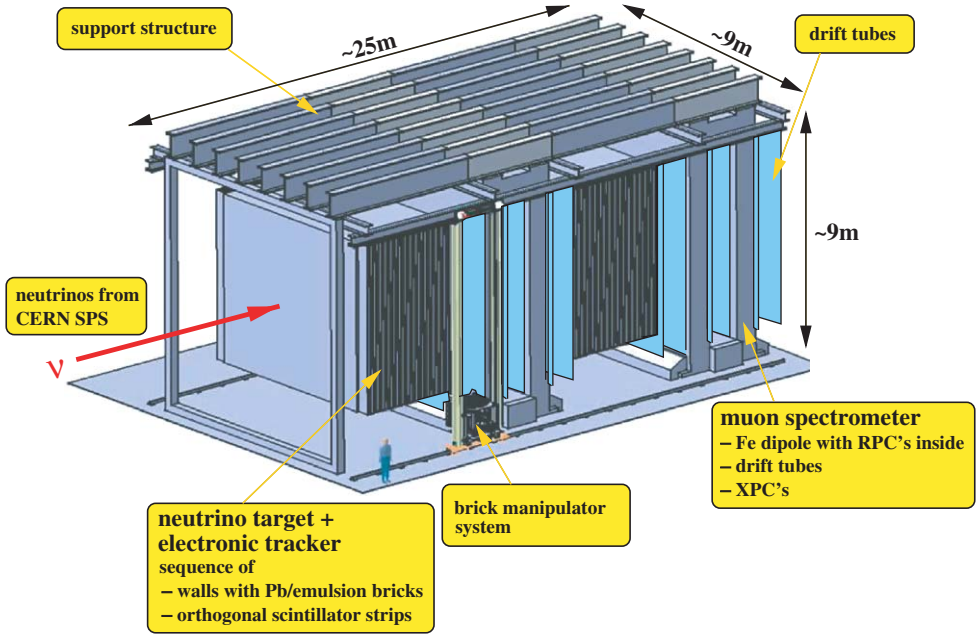

Fig. 1. The OPERA detector.

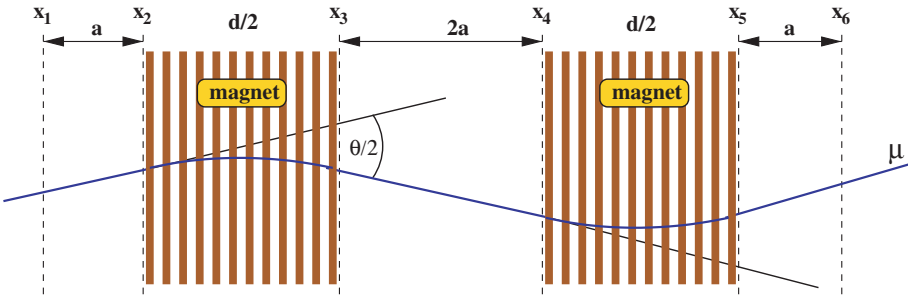

Fig. 2. Schematic layout of the OPERA muon spectrometer of one super module. The two iron core magnets are shown and the positions of the detector planes (dashed lines).

is given by the measured track coordinates x_i and the lever arm a.

$$\theta = \frac{x_2 - x_1}{a} - \frac{x_4 - x_3}{2a} + \frac{x_6 - x_5}{a} - \frac{x_4 - x_3}{2a} = \frac{1}{a}(x_2 - x_1 + x_6 - x_5 - x_4 + x_3). \quad (2)$$

In this detector configuration all 6 coordinate measurements enter with the same weight. Denoting the measurement error of one coordinate measurement by ε the contribution of the coordinate measurement error to the error of θ is

$$\Delta\theta_x = \frac{\varepsilon}{a}\sqrt{6}. \quad (3)$$

In addition, multiple scattering creates an error on the deflection angle

$$\Delta\theta_C = \frac{14\,\mathrm{MeV}}{pc}\sqrt{\frac{d}{X_0}} \quad (4)$$

where d denotes the thickness of the iron of both magnet sections and $X_0 = 0.0176\,\mathrm{m}$ is the radiation length of iron. The two errors are added in quadrature:

$$\Delta\theta = \sqrt{6\left(\frac{\varepsilon}{a}\right)^2 + \frac{d}{X_0}\left(\frac{14\,\mathrm{MeV}}{pc}\right)^2}. \quad (5)$$

A muon traversing the magnets is deflected by the total deflection angle

$$\theta = \frac{eBd}{p} \quad (6)$$

where $B = 1.55\,\mathrm{T}$ is the magnetic field in the iron at saturation. Hence, the momentum resolution of the spectrometer is given by

$$\frac{\Delta p}{p} \approx \frac{\Delta\theta}{\theta} = \frac{1}{eBd}\sqrt{6\left(\frac{\varepsilon p}{a}\right)^2 + \frac{d}{X_0}\left(\frac{14\,\mathrm{MeV}}{c}\right)^2}. \quad (7)$$

This expression describes the dependence of the spectrometer performance on the various relevant parameters.

For reasons of cost the iron thickness d is minimized. An iron thickness of $d = 1.2\,\mathrm{m}$ was chosen, such that the contribution of multiple scattering to the momentum resolution is

$$\frac{\Delta p}{p} = 0.21 \quad (8)$$

which is just small enough to reach the required momentum resolution also at high momenta. Again for reasons of cost and available space the lever arm a cannot be made longer than $a = 0.5\,\mathrm{m}$. With these parameters fixed, the required momentum resolution is reached if the coordinate measurement error amounts to

$$\varepsilon = 636\,\mu\mathrm{m}. \quad (9)$$

Hence, the structure and the size of the spectrometer are defined. The actual layout of the spectrometer has been worked out accordingly. Fig. 3 shows a simulation of the muon momentum distribution which is expected from the final spectrometer design demonstrating that the required momentum resolution is reached by this spectrometer design. The measurement error ε is composed of several errors: the intrinsic error of the drift time measurement, the error on the positioning of the signal wires within a drift tube module and the error on the alignment of the drift tube modules. All the contributions to the coordinate measurement error ε must be kept small enough, such that the combined error does not exceed 600 μm.

The intrinsic drift time measurement error of a drift tube will be about 300 μm. However, a detector plane will on average have more than two hits and will perform at least two measurements, therefore this error will reduce to 200 μm. Since OPERA is a low rate experiment, the individual wires cannot be aligned by tracks. However, the rates are sufficient to align 50 cm wide detector modules against each other. Thus, within a module the alignment precision must be achieved by precise mechanical positioning of the wires. Here a precision of 150 μm can be achieved. Consequently, for the overall alignment of the detector modules an error around 250 μm must be reached. In addition to alignment by tracks optical surveying will be applied to align the modules.

2.2. Tube arrangement and efficiency

The track detectors consist of 8 m long aluminum tubes with 38 mm outer diameter and 0.85 mm wall thickness. At the center a gold-plated tungsten wire of 45 μm diameter is strung.

In order to reach high detection efficiency and good rejection of the left–right ambiguity, a track must be measured by several adjacent detector layers. A detailed study shows that 3 layers are not sufficient. Too many tracks are lost in the walls of the tubes. However, with 4 layers enough redundancy is obtained. Even a distance of 4 mm between the tubes can be tolerated without any loss of performance. The optimal staggering was worked out by a Monte Carlo study using the expected angular distribution of the muon tracks produced. The resulting staggering is shown in Fig. 4. The tubes are arranged in two double layers. Within a double layer the tubes are packed as closed as possible. The two double layers are shifted against each other by 11 mm. The excellent performance of this tube arrangement is summarized in Table 1. For the reconstruction of a track, in two consecutive planes at least 4 hits are required. Table 1 shows, that even at a quite moderate single tube track efficiency of 85% (see Chapter 7.3.3), for 96.66% of the tracks 4 or more tubes are hit. In order to compute the track reconstruction efficiency, three requirements are made: at least 4 hits must be found in two consecutive planes, the track length in a tube must amount to at least 5 mm, and in case that a plane contains only one hit, the distance of the track to the signal wire must be larger than 3 mm to avoid the left–right ambiguity. The resulting track reconstruction efficiency is shown in Fig. 5.

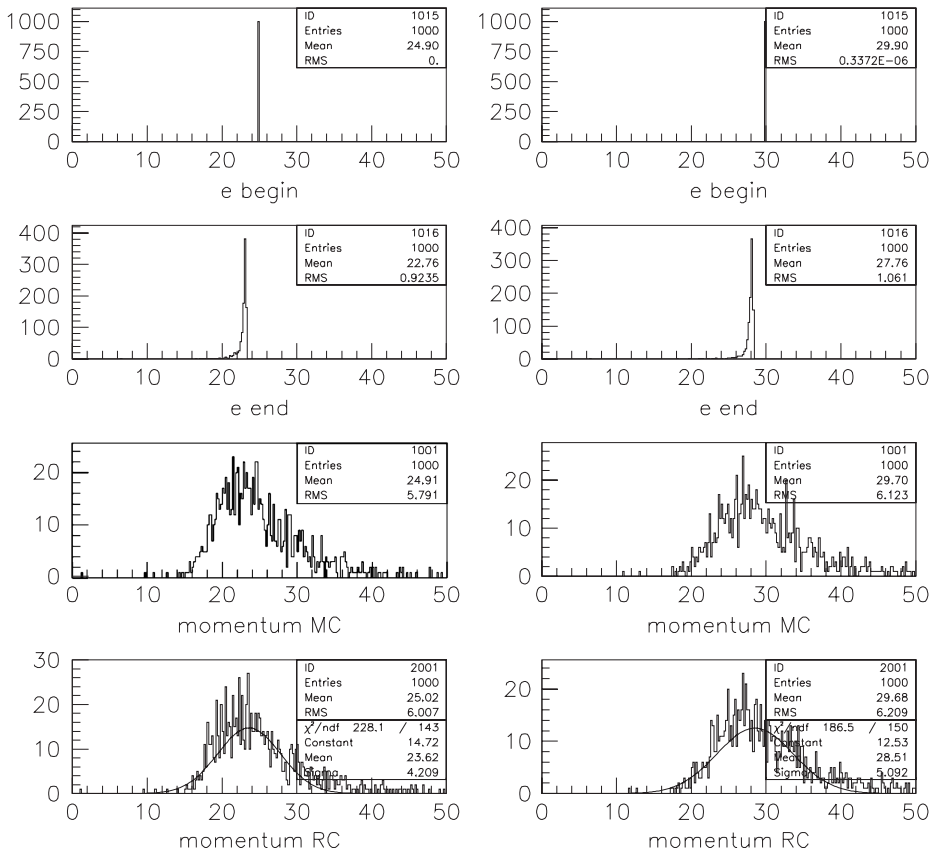

Fig. 3. Simulation of the muon momentum distribution measured by the OPERA muon spectrometer for muons with a momentum $25\,GeV/c$.

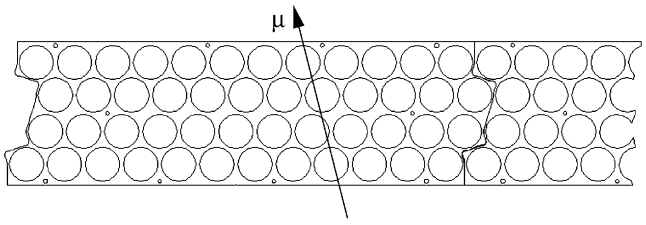

Fig. 4. Top view of tube arrangement and staggering.

Table 1
Frequency of observation of a number of hits in two consecutive planes depending on the single tube track efficiency

# Of hits	$\eta_{\text{tube}} = 100$ (%)	$\eta_{\text{tube}} = 90$ (%)	$\eta_{\text{tube}} = 85$ (%)
0	0.00	0.00	0.00
1	0.00	0.01	0.04
2	0.00	0.15	0.46
3	0.04	1.25	2.84
4	1.06	6.24	10.59
5	4.68	18.99	24.40
6	29.27	34.06	32.70
7	39.78	28.57	22.21
8	25.16	10.72	6.76

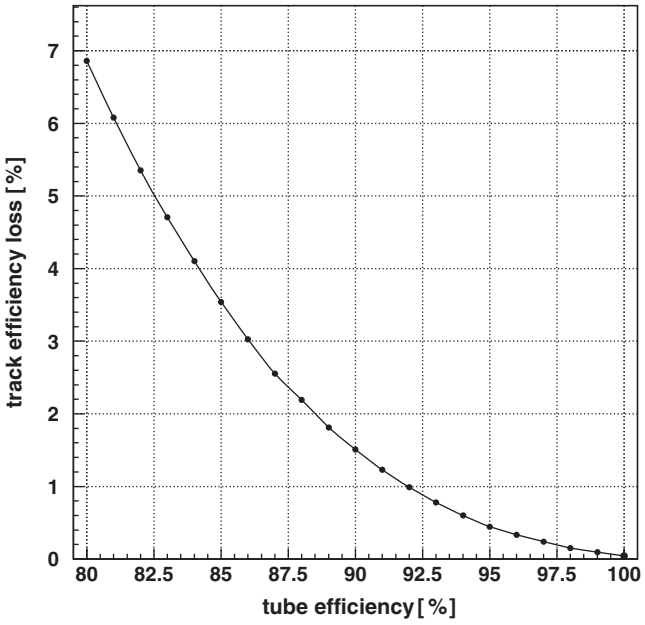

Fig. 5. Overall track reconstruction efficiency loss versus single tube track efficiency for an active tube radius of $r_{\text{active}} = 17.98$ mm, requiring a minimum track length of 5 mm.

The high track reconstruction efficiency demonstrates the excellent performance of the tube arrangement chosen. For a single tube efficiency of 90% only 1.5% of the tracks are lost.

3. The mechanical design of the precision tracker

From the specification of the precision tracker the mechanical design is a compromise to optimize the following requirements:

- Precision of wire positions better than 150 μm.
- Precision centering of the wires in the tubes.
- Mechanically secure HF-ground connection.
- Low resistance signal feed through covered by a Faraday cage.
- Minimum number of gas connections to reduce possible leaks.
- No contact of adhesives with the gas volume.
- No out-gassing materials.
- Staggering of the tubes to minimize ambiguities.

3.1. Mechanical layout

Each drift tube plane of the PT is built by 16 single modules, each module by 48 tubes. A schematic overview of a single module is shown in Fig. 6. The following chapter describes the mechanical design of the PT modules.

3.1.1. Tubes

The PT drift chambers consist of aluminum tubes (AlMgSi0.5) (Fig. 6(a)) similar to the ATLAS monitored drift tubes [6]. The specifications are summarized in Table 2. Straightness deviation 300 describes the maximum bending of a tube over a length of 300 mm, straightness deviation 1000 corresponds to a length of 1000 mm.

3.1.2. Bending

The 8 m long aluminum tubes are not perfectly straight. They are bent due to mechanical and thermal effects.

To study the influence of tube bending on the wire deflection and on the spatial resolution a GARFIELD simulation has been used. The results up to a bending of 2 mm using a wire tension of 190 g are shown in Fig. 7. The GARFIELD simulation shows that the maximal force perpendicular to the wire is in all cases less than $5 \times 10^{-6}\,\mathrm{N\,cm^{-1}}$ and the additional elongation is $<2 \times 10^{-7}$. Since the spatial resolution will be around 300 μm an additional deflection in the order of 100 μm is tolerable. Thus a tube bending up to 1 mm can be accepted.

The simulation was checked by an optical measurement on a tube prototype with two holes in the middle. This arrangement enables the observation of the wire during switching the high voltage while bending the tube up to 1 mm. Within an accuracy of 100 μm no visible wire deflection has been observed. From this study we conclude, that a deviation from a perfectly straight tube up to 1 mm can be safely tolerated and that the signal wire does not need any mechanical support over the total tube length of 8 m.

3.1.3. Perforated aluminum sheets

Instead of aluminum plates as described in the ATLAS muon drift tube chamber design [6] we are using perforated aluminum sheets (Fig. 6b) to fix the tubes. The tubes are arranged in 4 rows with 12 tubes. The thickness of the perforated aluminum sheets is 8 mm. The distance of the sheets is about 1 m along the tubes. In this way small straightness deviations of the tubes will be corrected.

The side shape of the perforated sheets results from the necessity to mount the single modules side by side with the same tube distance as inside a module. No change in the tube distance should occur along a Precision Tracker wall.

The accuracy of the hole position in the perforated aluminum sheets is ±50 μm. The oversize of the drill hole diameter is in a range from 100 μm up to 150 μm, space needed for fitting the tubes into the sheets and for the epoxy adhesive. Taking into account the tube production tolerances misalignment of the tube center is 350 μm in the worst case as shown by Table 3.

3.1.4. End plates

Different from the ATLAS design [7] the PT drift tubes are not closed by single end plugs. Special end plates (AlMgSi0.5) (Fig. 6 top end plate c, bottom end plate d) cover the ends of a drift tube module.

The tube ends fit into blind holes of the end plate. The position of the blind holes and the side shape are the same as at the perforated aluminum sheets. The thickness of the top end plate is 25 mm, due to the blind holes and space for the wire support, while the bottom end plate has 30 mm accounting for the tolerances of tube length.

Fig. 8 shows a sectional drawing of a top end plate. Two grooves are milled in the blind holes. The outer one takes an o-ring (Fig. 8 part e) for sealing and to separate the mounting adhesive from the gas volume. The inner one takes a sharp-edged copper–beryllium spiral spring (Fig. 8 part f) to get a mechanical secure HF-ground connection. The elastic spiral will scratch the aluminum tube and destroy the oxide film to guarantee a safe grounding.

The plastic insert (Fig. 8 part k) acts as chamfer to reduce the forces during fitting the tube into the blind hole of the end sheet. It protects o-ring and spiral spring against damage during assembly. In addition the insert defines the stop position to prevent the closing of the gas channels by the tube wall.

The 48 tubes of a module have a serial built in gas connection. The hose connection (Fig. 6 part i) for the gas supply of the module is realized at the bottom end plate (Fig. 6 part d). Milled gas channels (Fig. 8 part g) between the blind holes connect the tubes. The cross-section is

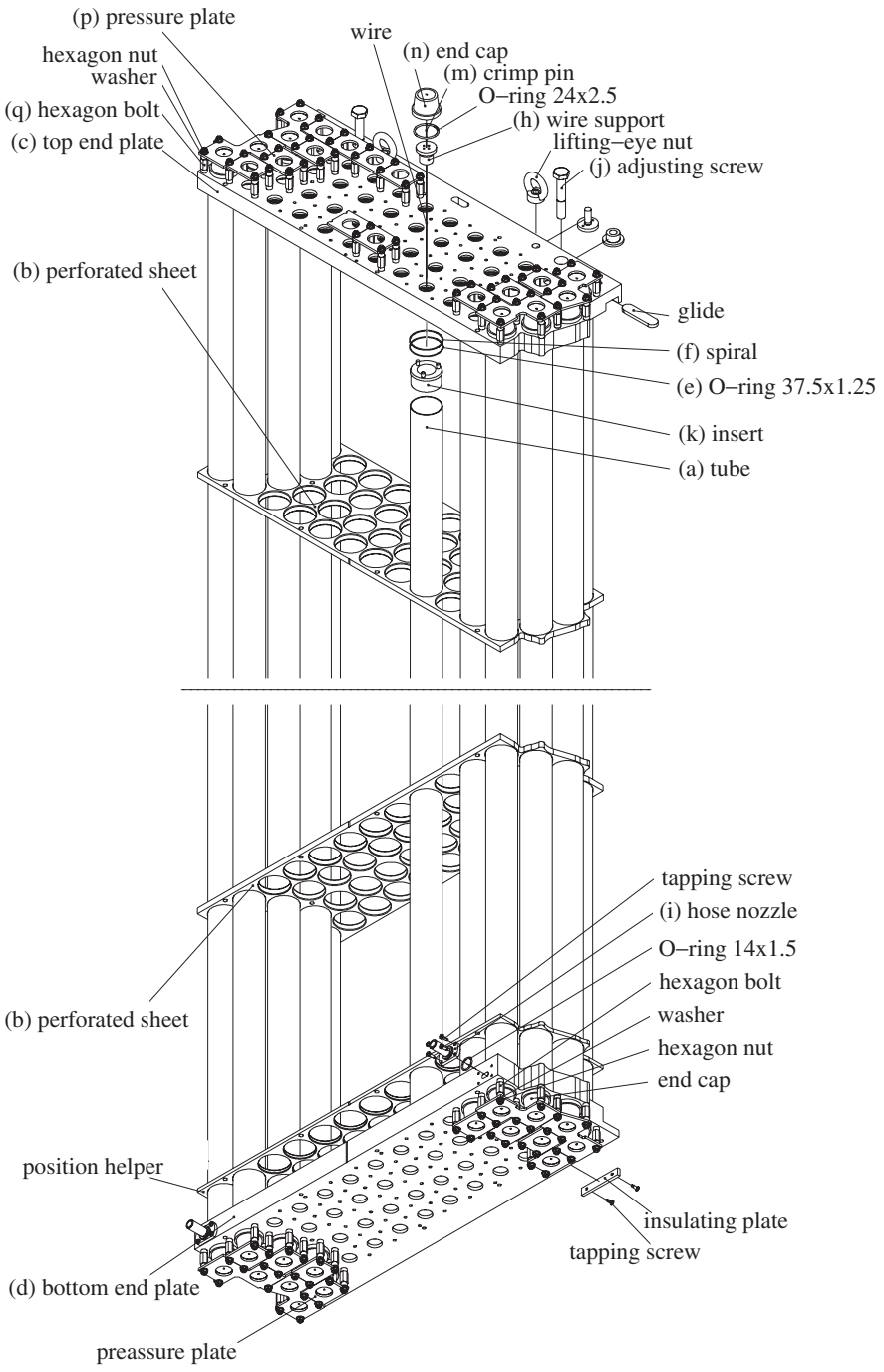

Fig. 6. Schematic view of a PT module.

Table 2
Technical data of a single tube

Description	Value (mm)
Length	7900^{+0}_{-5}
Outer diameter	$38.00^{+0}_{-0.15}$
Wall thickness	$0.85^{+0}_{-0.15}$
Straightness deviation 300	0.15
Straightness deviation 1000	1.00

65 mm^2. At both tube ends only one o-ring per tube is needed for sealing the gas flow from tube to tube. Pipes with a connecting system are not necessary. If the o-ring sealing fails the outer glue will act as sealing. Therefore we use a glue without out-gassing (AW103).

A groove at the bottom side of the top end plate acts as the suspension. The groove fits into a rail, which is mounted at the magnet. Two screws (Fig. 6 part j) tilt the module for vertical alignment with a pendulum.

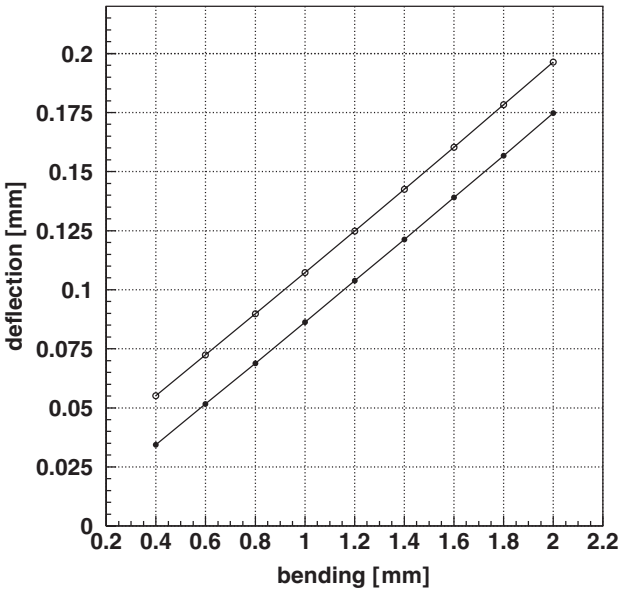

Fig. 7. GARFIELD simulation of the wire deflection by tube bending. The closed circles show the additional wire deflection by tube bending at an operating voltage of 2.4 kV. The open circles show the same simulation with an additional wire shifting of 200 μm (due to mispositioning of the sense wire).

Table 3
Maximum misalignment of the inner tube center

Deviation originates from	Maximum deviation (μm)
Outer tube diameter	75
Wall thickness	150
Oversize of the drill hole	75
Accuracy of the hole position	50
Total	350

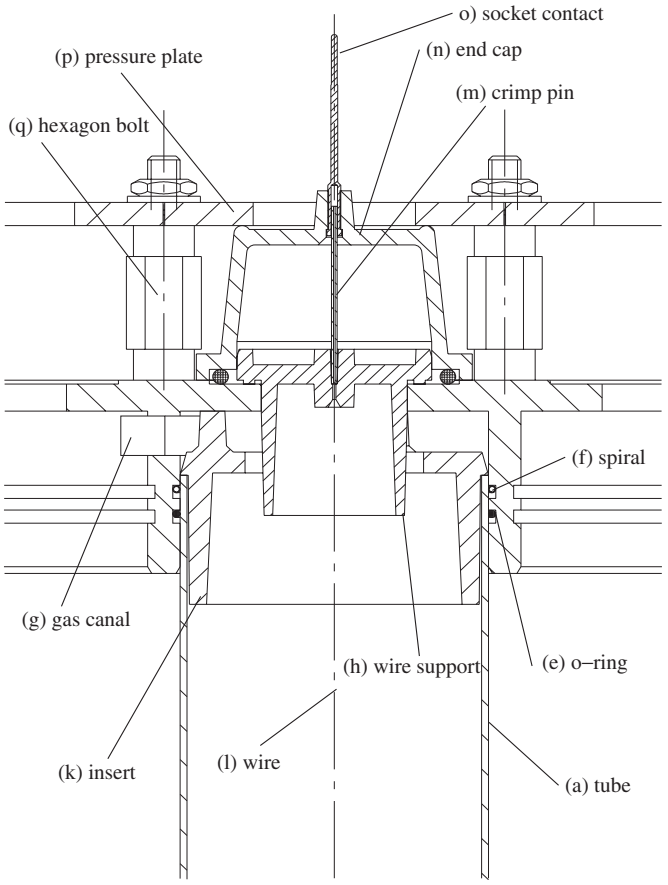

Fig. 8. Sectional drawing of a top end plate.

Table 4
Technical data of the CWF-wire

Outer diameter	45 μm
Collapse load	400 g
Elastic limit	288 g
Tension	186 g

3.2. Signal transmission

3.2.1. Wire

As the wires (Fig. 8 part l) will not have any centering support between the bottom and the top, mechanical stability at the HV limits is important. In order to operate after large temperature variations during transport of the modules, the thermal expansion of the aluminum tubes should not increase the tension over the elastic limit. On the other hand the tension has to ensure, that wire deflections due to electrostatic effects will not occur, or be negligible (see also bending).

The test results of several wires are summarized in Ref. [8]. Table 4 summarizes the data of the chosen gold plated tungsten wire from CWF.[4]

The nominal value of the tension of 186 g is big enough to ensure only negligible wire position deviations due to electrostatic forces (see also bending). On the other hand the tension will not exceed the elastic limit in case of an additional load due to a temperature increase. Assuming a 40 K temperature increase the additional load will be around 40 g.

3.2.2. Wire support

18 mm diameter holes are on the outer sides of the end plates. They are centered to the blind holes and take the wire support (Figs. 6 and 8 part h). The wire fits through a hole of 0.4 mm. Along 2.5 mm the diameter increases to 0.7 mm to take the crimp pin (Figs. 6 and 8 part m) with an outer diameter is 0.7 mm and inner 0.2 mm. The crimp pin hole of 0.2 mm centers the wire.

In this way the position of the wire depends only on the tolerances of the hole position (50 μm) for the wire support and the tolerances of the wire support itself (<100 μm) including the wire positioning by the crimp pin. Even in a

[4]California wire factory.

worst case of adding up all tolerances the wire position is known with an accuracy better than 150 μm concerning the module.

The wire support is produced by injection moulding. For the prototype a turned version of the wire support is in use.

3.2.3. Crimping

Copper crimp pins on both sides of the tube fix the wire. The outer diameter is 0.7 mm the inner 0.2 mm. The length of the crimping is about 10 mm. The crimp tool consist of a standard crimp tool[5] with modified jaws.

The crimping is defined by the remaining thickness of the crimp pin, independent of the necessary force. Fig. 9 shows the collapse load of different crimps as a function of the remaining thickness of the crimp pin. There is no crimp, if the remaining thickness of the crimp is bigger than 0.51 mm. The wire slips in the region 0.48 mm up to 0.50 mm. The production tolerances of the crimp pin are the reason for different tensions at the same remaining thickness. Decreasing the remaining thickness lower than 0.48 mm the collapse load of the wire was always reached before the crimping fails. For safety reasons a remaining thickness of 0.44 mm was chosen for crimping of the prototypes.

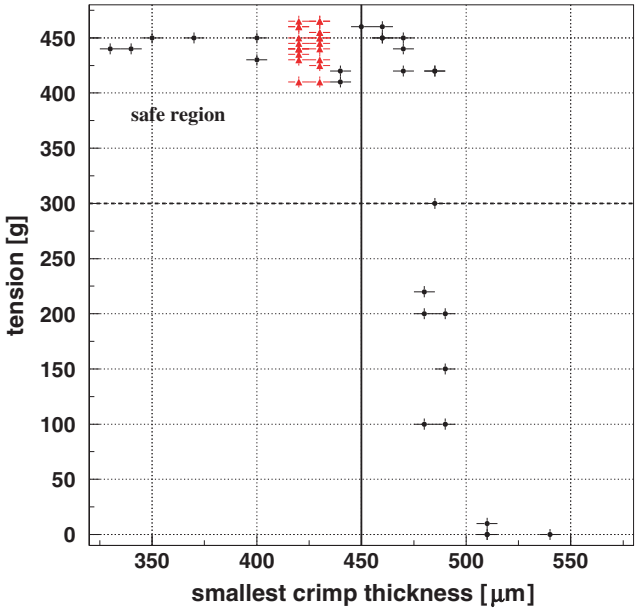

Fig. 9. Crimping collapse load vs. remaining thickness of the crimp pin after crimping.

3.2.4. End cap and signal feed through

The end cap (Figs. 6 and 8 part n) closes the gas volume and feeds the signal outside the tube to the HV-board with a socket contact (Fig. 8 part o). An o-ring seals between end plate and end cap. The socket contact is pressed in the end cap. Pressure tests shows tightness up to 4 bar. The used end cap is also a turned version of the designed moulded one.

Pressure plates (Figs. 6 and 8 part p) squeeze down the end cap with hexagon bolts (Figs. 6 and 8 part q). By this way an individual access to each single wire support is possible. In addition a coarse Faraday cage is realized at the tube end.

4. Assembly of modules

4.1. Tube preparation

For a high efficiency of the PT the gas volume must be oil and lubricants free. As the tubes are extruded pipes, lubricants are used during extrusion which are not totally removed by the cleaning procedure of the supplier. An additional purification is necessary. Cylindrical sponges drenched in Isopropyl alcohol are pushed by cleaned compressed air through the tubes several times until no contaminations are visible. Afterwards the tubes are flushed with air to get free of the Isopropyl alcohol, whose vapors could oxidize the inner surface in combination with air humidity. Both tube ends are covered with caps during storage to avoid any new contamination.

[5]Thomas and Betts WT-4454G.

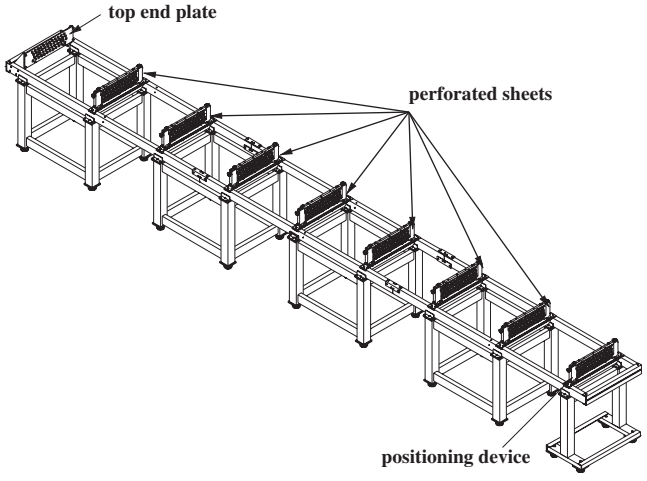

Fig. 10. Mounting table.

4.2. Mounting table

In order to achieve the required precision in positioning the wires, a possible bending or twisting of the modules has to be minimized. High precision tools have to guarantee the proper position of all parts during assembly of the module. The top end plate, the seven perforated aluminum sheets and the positioning device at the bottom of the module are mounted on a special frame, the mounting table, Fig. 10. The position of the aluminum sheets is manually adjustable in all 6 degrees of freedom (rotation and translation). A laser tracker was used to measure and adjust the position of the sheets relative to the top

end plate. The accuracy of the laser tracker amounts to $\pm 10\,\mu m$.

4.3. Glueing

A single tube at a time is slid through the perforated aluminum sheets until it reaches the front of the top end plate. Before fitting the tube in its final position, the "epoxy adhesive" for its connection to end plate and perforated sheets is applied. Turning the tube results in bonds over the full circumference. Afterwards the tube is pressed into the top end plate. The force needed is reduced by the insert at the tube end, which in addition defines the stop position such that the flow through the gas channels is not affected. This sequence is repeated until all 48 tubes of a module are in place.

After curing the bonds overnight, the bottom end plate can be mounted. All 48 tubes have to be pressed into the blind holes of the bottom plate at the same time. The unglued positioning device at the bottom of the module serves to center the tube ends to their holes.

Glue is applied only to the tubes at the outer sides surface of the module because application in between would need complicated tooling due to the limited space. This does not affect the suspension of the modules as their load is only taken by the top end plates.

The force needed to press the tubes with the inserts into the plates is a factor of about 50 higher than in the case of a single tube. It is mediated by a gadget (see Fig. 11) consisting of a pressure plate behind the bottom end plate, pull rods and a dedicated frame encompassing the last perforated sheet at the bottom side, which takes over the pressing forces. The nuts on the pull rods are screwed in a step by step procedure in order not to fill the end plate. Their stop position defines the penetration depth of the tubes into the end plate.

4.4. Wiring

The wire is threaded through the 8 m long tube by means of compressed air acting on a cushion with the inner tube diameter, which can be compressed to insert it through the narrow holes of the end plate. After fixing the wire on one side by crimping a weight of 186 g stress the wire on the other side and the second crimp is applied.

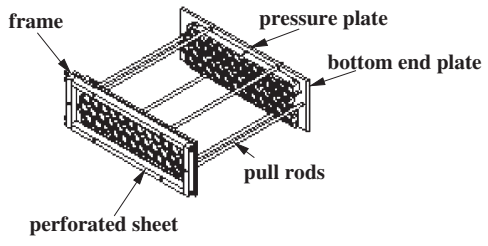

Fig. 11. Gadget for mounting the bottom end plate.

4.5. Wire tension

To check the wire tension after crimping, it has to be measured carefully. For quality control during mass production a fast and simple method is required.

The wire tension measurement is done by applying a magnetic field in the middle of the tube and producing a mechanical deflection onto the wire induced by a short (3.75 ms) square pulse of high current (153 mA). By determining the time between the start of the wave pulse at the magnet and its arrival at the magnet with the original polarity, after two reflections at the tube ends, the wire tension can be calculated. The advantage against previous methods described in literature [9–14], is the robust ability to complete a measurement in a few seconds. Other methods suffer from the disadvantage that in searching for resonant frequency, one must scan many frequencies in the range where is the resonance is expected. This is time consuming and for large wires there is a danger of mistaking a higher harmonic for the fundamental, thus greatly overestimating the wire tension. These effects can be avoided by the described method.

The wave velocity v is related to the two equations:

$$v = \frac{2l}{t} \quad \text{and} \quad v = \sqrt{\frac{Tl}{m}} \tag{10}$$

where l denotes the wire length, T is the tension, t the period and m the wire mass. Replacing the mass m by the density ρ and the wire diameter d we get a relation for the wire tension:

$$T[N] = \rho\pi d^2 \frac{l^2}{t^2}. \tag{11}$$

The used apparatus is shown in Fig. 12. A measured result is shown in Fig. 13. To suppress noise peaks the scope average mode has been used. The result in the given example is 69.4 ms. The accuracy of this method is limited by the display resolution of the used scope, thus for our case better than 2%.

5. Tests of the assembly materials

To avoid efficiency loss due to interferences with emissions of the used materials in the detector out-gassing tests of these materials were done. The used setup for these studies is shown in Fig. 14. The OPERA gas mixture Argon and CO_2 in a ratio of 80% and 20% was used. The gas flow was defined by the flow meter, the valves were used for closing the gas flow completely. As detector acts a brass drift tube with a length of 1 m, an inner diameter of 36 mm and a gold-plated tungsten sense wire with a diameter of 45 μm. The drift tube was operating with cosmics. A test volume with the materials to investigate was included into the gas flow in front of the drift tube. The efficiency was measured by the ratio of the hits by coincidence of the scintillators and the drift tube and the number of hits by the coincidence of both the scintillators.

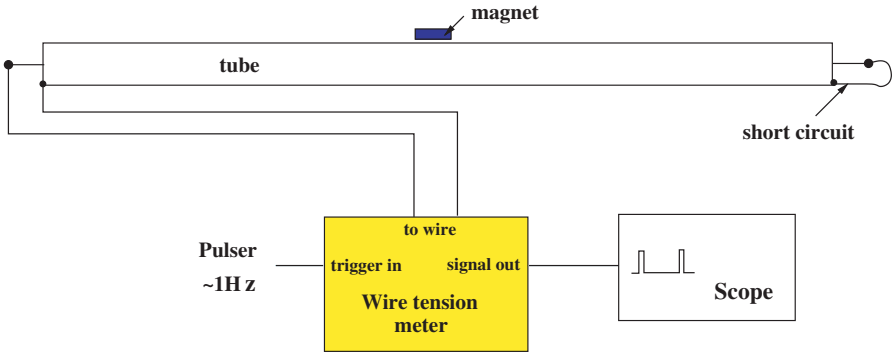

Fig. 12. Schematic view of the tension-measuring apparatus.

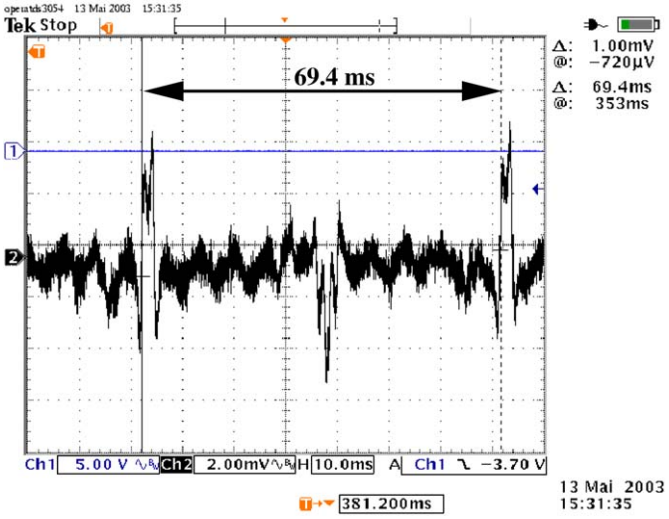

Fig. 13. Tension measurement waveform from 8 m OPERA tube.

The efficiency study was going over several days with different gas flows. Starting with a flow of 4 V/h (volume means the drift tube volume) the flow was decreased to 0.2 V/h and after some hours stopped completely as shown in Fig. 15. The efficiency was measured over this time and the flow was increased again up to 0.2 V/h. To find out the quality of the used materials an inverse quality factor K was calculated:

$$K = -\frac{d\eta}{\eta t S}\left[\frac{\%}{[d][m^2]}\right] \tag{12}$$

with $d\eta/\eta$ as efficiency loss, S as active surface of the material in [m^2] and t as the given time in [d]. The smaller the value of K is the better the quality concerning the outgassing. The results are summarized in Table 5. Except for the Araldite glue AW106 the tested components have negligible influence on the efficiency at the nominal OPERA gas flow of 1 V/72 h. As glue we therefore use Araldite AW103 instead of AW106 due to negligible outgassing as described in Ref. [16].

6. The front end electronics

The OPERA front end electronics consists of four parts: the distribution board, the amplifier & discriminator board (ADB), the support board and the TDC board. Except for the TDC board which is a development of the University of Rostock all boards are developed by the University of Hamburg. The requirements for the front end electronics are:

- Massive grounding.
- Safe signal transmission.
- Ability for remote controlling and monitoring.
- Low cost system.

Such boards which fulfill all these requirements will be described in the following subsections.

6.1. HV-distribution-board

The PT distribution-board shown in Fig. 17 is developed to supply the drift tubes with high voltage and to transmit the analog signals from the tubes and to provide the low voltage to the ADB. One board covers twelve channels in one layer of a module (see 3.1) thus we need 792 boards in total. The board is designed as multilayer board with six layers. That's the requirement to feed the grounds for digital, analog and high voltages separately to optimize the grounding. By the same reason the board is fixed to the tubes by a massive ground connection made of brass bolts and copper beryllium nuts. The HV is connected by an 1 MΩ resistor R2 (Figs. 16 and 17) to each sense wire. The coupling of the signals is done with an capacitor C2 of 1 nF for each channel. To avoid influences by noise catching on the long HV cable there is a filter elements consisting of a capacitor C1 of 1 nF and a resistor R1 of 1 kΩ on the HV input. The low voltages for the amplifier and discriminators are daisy chained from board to board with standard power lines. This low cost supply avoids also crosstalk from signal lines to the power lines over long distances. For the HV we spend one cable per board to have the possibility to switch off the boards separately if necessary.

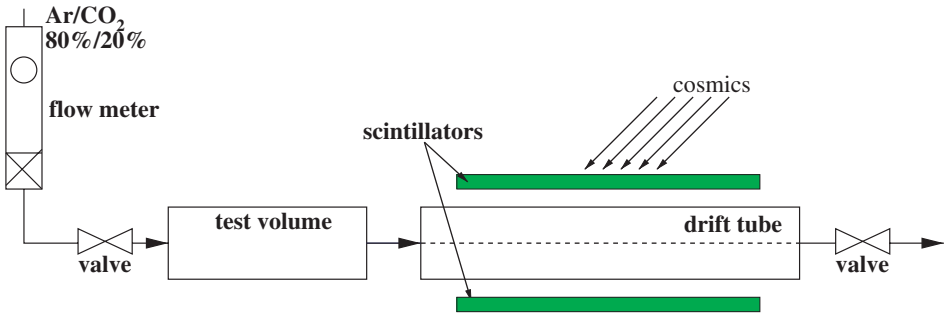

Fig. 14. Test setup for the out-gassing measurements. The test volume was filled by the material used in the drift detector.

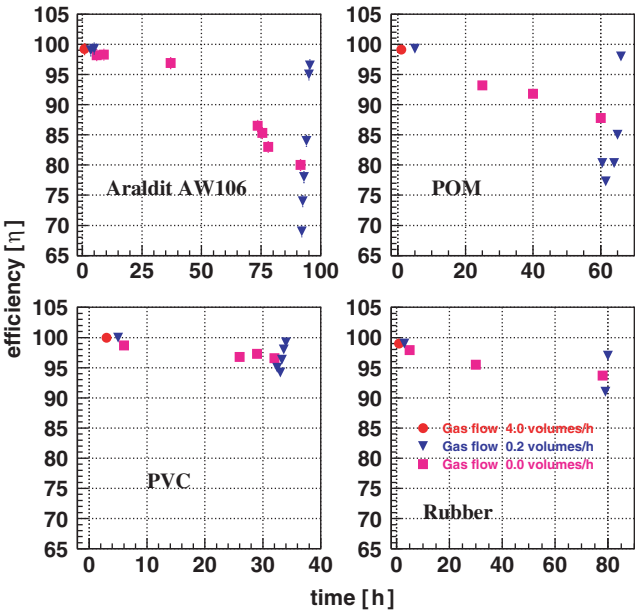

Fig. 15. Long time efficiency measurements for different materials and for different gas fluxes (the circles mark a flow of 4 V/h, the triangles mark a flow of 0.2 V/h and the boxes mark a flow of 0 V/h).

Table 5
Inverse quality factor K of the tested material

Tested material	Surface (m^2)	K (%/day × m^2)
POM shavings	1.40	0.06
Rubber rings	0.25	0.12
PVC pieces	0.30	0.14
Araldite glue AW106	0.01	7.5

The signal transmission to the ADB and the power supply is done by three 20 pin connectors.

6.2. Amplifier and discriminator board

The amplifier and discriminator board is carrying the amplifier, the discriminator and circuits for threshold setting, temperature monitoring and test pulse generation on board. It is designed equivalently to the distribution board as six layer board to optimize the grounding. To avoid self oscillation behavior analog and digital parts are strictly separated. The analog part mainly consists of the amplifier. As amplifier we are using the forward muon detector amplifier of the L3 experiment which is described in Refs. [17,18]. It is a low power two stage four-fold hybrid linear amplifier with feedback stabilized current gain and an amplification factor of $2 \times 60\,\mathrm{mV}/\mu\mathrm{A}$. The first stage has an extensive input protection network against discharges up to 3 kV. The L3 amplifier is designed as bootstrap amplifier and guaranties a sharp leading edge. The resistive feedback produces a low dynamic input impedance. The second stage is a post amplifier with a balanced complementary output signal AC coupled on the first stage. The main specifications are listed in Table 6. As discriminator acts the low-power, ultra-high-speed comparator MAX963 from the company MAXIM described in Ref. [19]. With its internal hysteresis of 3.5 mV a clean switching is given. The propagation delay is 4.5 ns. The differential output signals of the circuit are transformed by a resistor network consisting of R6 and R7 into LVDS signals, which drive the TDC input stage. The coupling to the amplifier is done by a 0.1 μF capacitor C3 (Fig. 16). Amplifier and discriminator are placed on the same board. This has the advantage that only digital signals are transmitted over long distances to the TDC and the disturbing noise catching can be avoided. The cable to the TDC can be unshielded as well.

The threshold settings can be controlled individually for each channel by means of the support board. This gives the possibility to switch off hot channels by increasing the threshold value. The threshold voltage V_{th} will be supplied via the resistor R5 as shown in Fig. 16. Both the resistors R4 act to define the potential on the discriminator input. Furthermore the test pulses are produced on board for odd, even and all channels for operating tests, calibration and crosstalk measurements. For one board one channel for temperature monitoring is spent. The sensor can be placed via maximum 10 m long lines somewhere in the spectrometer. The controlling and monitoring is done by the support board via an I^2C like bus connection as part of

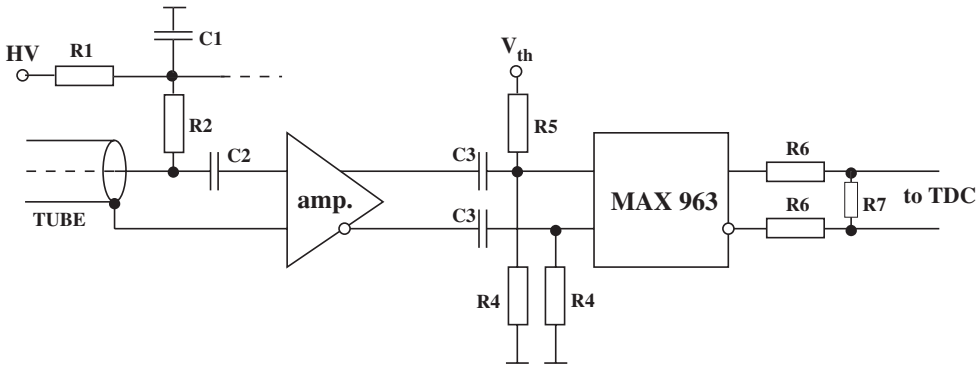

Fig. 16. Scheme of one electronic channel. The tube signals will be amplified by the L3 amplifier. The AC coupled discriminator produces the digital signal which is shaped by a resistor network to define the level for the TDC input.

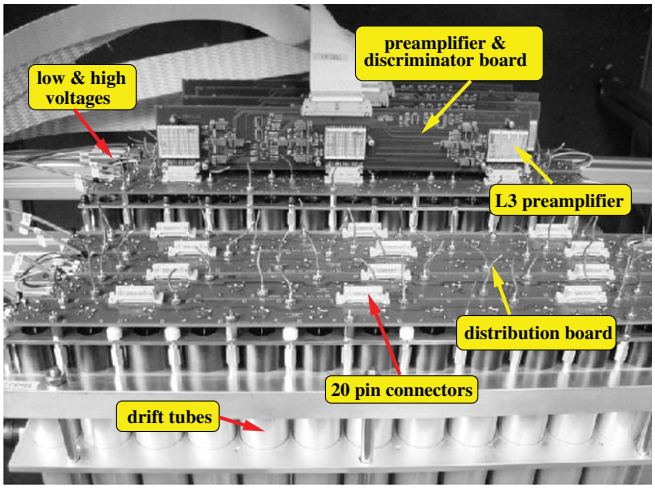

Fig. 17. Photo of the used distribution and amplifier and discriminator boards in the test setup.

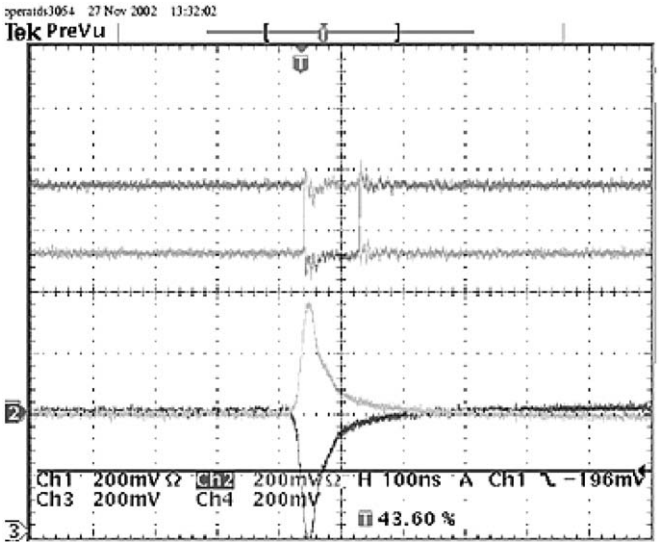

Fig. 18. Plot of the analog and digital output signal measured with a Fe^{55} source.

Table 6
Specification of the L3 amplifier

V_{CC}	5.0 V ± 5%
Gain	2 × 60 mV/μA
Rise time	6 ns
Output impedance	2 × 50 Ω
Output drive	>20 mA
Output asymmetry	<5%

the signal output cables. An analog and digital output signal taken with a Fe^{55} source is shown in Fig. 18.

6.3. TDC system and support board

The TDC system is developed by the University of Rostock in cooperation with DESY Hamburg. This system will have a dynamic range of 3.2 μs with a LSB of 1.6 ns. In addition the OPERA TDC has the possibility to measure the pulse width and store it in three classes (<15.5, 12.5–81.25, >81.25 ns). Since at this time no OPERA TDC is available because the development is ongoing we use the VME TDC V1190A from CAEN. It is a 6U Multi-Hit/Multi-Event TDC with 128 independent time to digital conversion channels. We use it with a dynamic range of 52 μs with a LSB of 100 ps [20].

For controlling and monitoring the ADB the support board was developed by the University of Hamburg. This board is responsible for setting the threshold and the test pulse pattern (odd/even/all channels). The generation of the test pulses is done on the ADB directly. For each ADB one measurement point for temperature is foreseen. The support board can be used with a CAN bus system.

7. Results

7.1. Gas tightness

The total gas volume of the entire detector amounts to 80 m^3. For reasons of cost and logistics, the gas cannot be

exchanged more often than once per 3 days. This condition poses strict requirements on the gas tightness of the drift tubes. In order to estimate the leak rate, a drift tube module was filled with a gas mixture of Ar/CO_2 at an initial overpressure of 150 mbar. Taking variations of temperature and atmospheric pressure into account, after 6 weeks no noticeable pressure decay was observed within the measurement error of a few mbar. After removing the gas supply and closing the detector, for 10 days the detector efficiency was still unchanged. This showed that the detector is sufficiently gas tight.

7.2. Signal attenuation

The read out electronics is placed on top of the drift tubes. The electronic signal of a particle which traverses a tube near the bottom, has to travel over 8 m through the tube until it reaches the amplifier on top. Therefore it is important to measure the attenuation of the signal introduced by the signal transmission. For this purpose into an 8 m long tube 15 equidistant tiny holes were drilled and closed with adhesive tape. Through these holes the gas inside the tube was irradiated by a Fe^{55} source. For each hole i, located at a distance from the amplifier $x_i = i\ 0.5\,\mathrm{m}$ with $i = 0-15$, the pulse height U_i was measured. The observed pulse heights are shown in Fig. 19. They are well described by an exponential

$$U_i = U_0 \exp -\frac{x_i}{\lambda}.$$

The attenuation lengths λ was obtained by a fit of an exponential to the data and amounts to

$$\lambda = (32.1 \pm 0.2)\,\mathrm{m}.$$

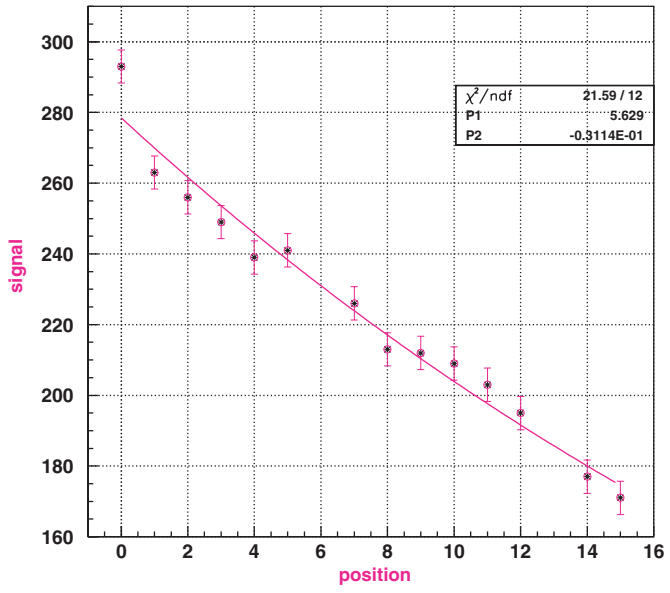

Fig. 19. Pulse heights measured with a Fe^{55} source at positions $i = 0-15$, which are located at a distance from the amplifier $x_i = i \times 0.5\,\mathrm{m}$. The curve is an exponential fitted to the data.

For this measurement the signal wire was terminated with the wave resistance at the far end in order to avoid reflections, however, actually the tubes are operated without termination to reduce signal attenuation. We conclude that the attenuation of the signal is small enough to enable a safe operation over the full drift tube length of 8 m.

7.3. Measurements with the prototypes

To study the performance of the drift tube detector and the associated front end electronics, short and large prototypes were built. The small prototype consists of 1 m long tubes. Two modules with 48 tubes are placed on top of each other. Hence this tube arrangement consists of eight layers of drift tubes. They are covered on top and bottom by large scintillators and a suitable lead layer for triggering by minimum ionizing cosmic ray particles. The large prototype consists of only four layers of 8 m long tubes and is covered only at the end by large scintillators to have a signal transmission over almost the whole length to have possible run time and attenuation effects included into the measurements. Both prototype versions are equipped with the final high voltage boards and the final amplifier boards. The readout is performed via the CAEN V1190A TDC. The drift tubes were operated with an Ar/CO_2, 80/20 gas mixture. Measurements with this gas mixture for the ATLAS monitored drift tubes are published in [21–24]. The high voltage was varied between 2.1 and 2.4 kV. The trigger rates were around $15\,s^{-1}$ for the small prototype and $2\,s^{-1}$ for the large prototype. The data thus collected were analyzed by a reconstruction program described in [25]. It reconstructs straight tracks with a "line to circles" fit in an iterative procedure and simultaneously generates the r–t relation which are updated each iteration. The r–t relation (Fig. 20) converts the measured drift time into a track coordinate. The spectrum of the TDC times is shown in Fig. 21. The maximal drift time is about 1.3 μs. In addition the spatial resolution and the tube hit and track efficiencies are computed.

7.3.1. Wire alignment

An advantage of the used track reconstruction software is the alignment of the wire positions. The actual positions of the signal wires were determined by the track reconstruction and compared with the nominal values of the wire positions. The measured deviations of the actual position from the nominal position have a Gaussian distribution with a rms of 50 μm. This result reflects the high mechanical precision of this drift tube detector design.

7.3.2. Spatial resolution

To get the mean resolution of the single drift tube the residuals, that means the difference of the fitted and the measured drift distance, will be saved for each event. The r.m.s. value of the residual distribution yields the spatial resolution of the drift tube. Fig. 22 shows the spatial

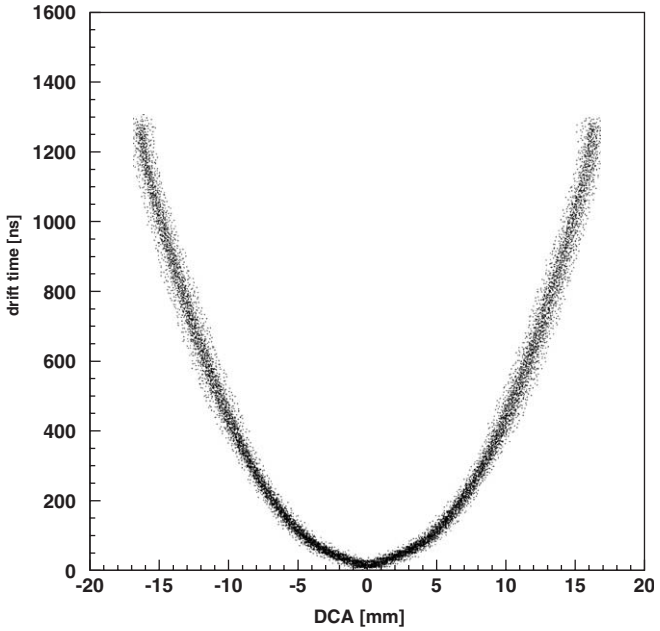

Fig. 20. The r–t relation for a drift tube operated with an Ar/CO_2 80/20 gas mixture at an operating voltage of 2.3 kV and a discriminator threshold of 50 mV.

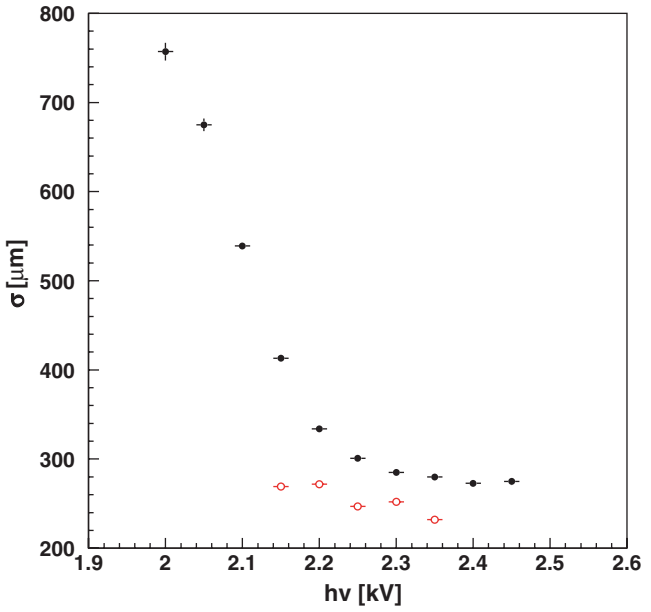

Fig. 22. Spatial resolution of the small (closed circles) and the large prototype (open circles) averaged over all track positions versus high voltage for a discriminator threshold of 50 mV corresponding to an input current of 0.5 μA.

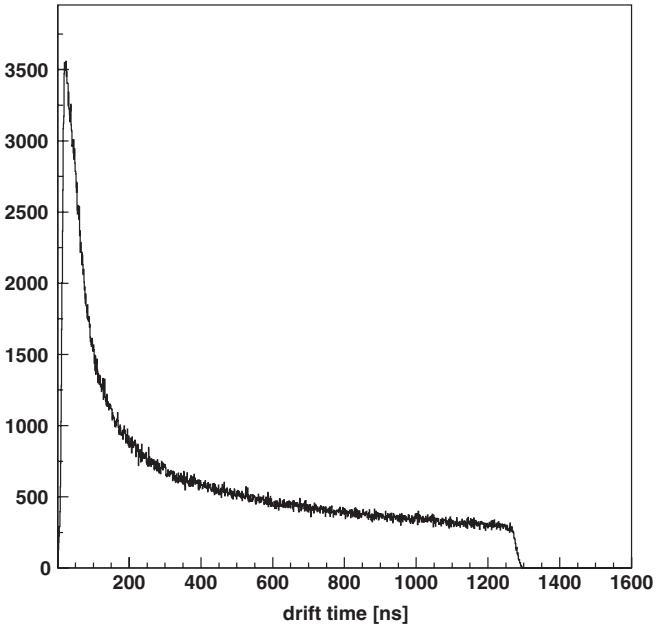

Fig. 21. Distribution of the measured TDC times for an operating voltage of 2.3 kV and a threshold voltage of 50 mV. The maximal drift time is 1.3 μs.

resolution for a coordinate measurement as a function of the high voltage applied. The closed circles show the measurement with the small prototype, the open circles show the results with the long prototype. A discriminator threshold of 50 mV was chosen, which corresponds to a current of 0.5 μA at the input of the amplifier. This threshold enables a good suppression of noise and cross talk signals. Above a high voltage of 2.3 kV a spatial resolution of $\sigma = 285\,\mu m$ for the small prototype and $\sigma = 269\,\mu m$ for the large prototype is reached. The spatial resolution for the small prototype corresponds to a track resolution of $\sigma_{track} = 285\,\mu m/8$ layers $= 100\,\mu m$ for the small prototype and $\sigma_{track} = 269/4$ layers $= 135\,\mu m$ for the large prototype respectively. Actually the drift tubes can be safely operated up to a high voltage of 2.4 kV, without noticeable after-pulsing. The good spatial resolution shows that the electronics chain developed does not deteriorate the intrinsic spatial resolution of the drift tubes and is adequate for our demands. Compared with the total resolution of $\varepsilon = 600\,\mu m$ calculated in Eq. (9) of Section 2.1 we can allow nearly 450 μm for misalignment of the modules if we use a upper limit for the track resolution of $\sigma_{track} = 150\,\mu m$ and add up the errors absolutely.

7.3.3. Detection efficiency

The reconstructed tracks traversing the 8 drift tube layers of the short prototype provide an excellent possibility for a precise determination of the detection efficiency of the drift tubes. The drift tube under study is excluded from the track reconstruction. After a track, which passes through this particular tube, is reconstructed it is checked whether this tube has fired. The ratio of fired to not fired gives the single tube hit efficiency η. Fig. 23 shows the single tube hit efficiency η for the small prototypes. At the operating voltage of 2.3 kV $\eta > 98\%$. In Fig. 24 the hit efficiency distribution over the tube radius for the small prototype is shown. Excluding the outer 3 mm of the drift tube η amounts to 98.96%, independently of the

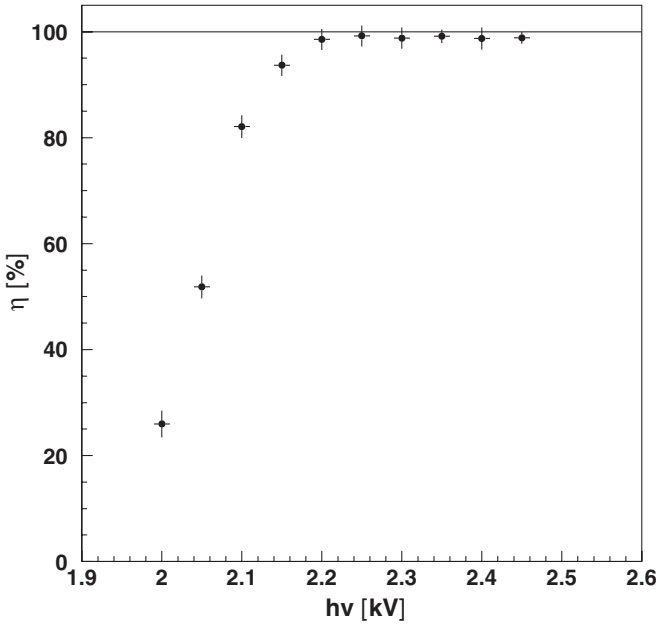

Fig. 23. Single tube hit efficiency dependent on high voltage at a threshold voltage of 50 mV.

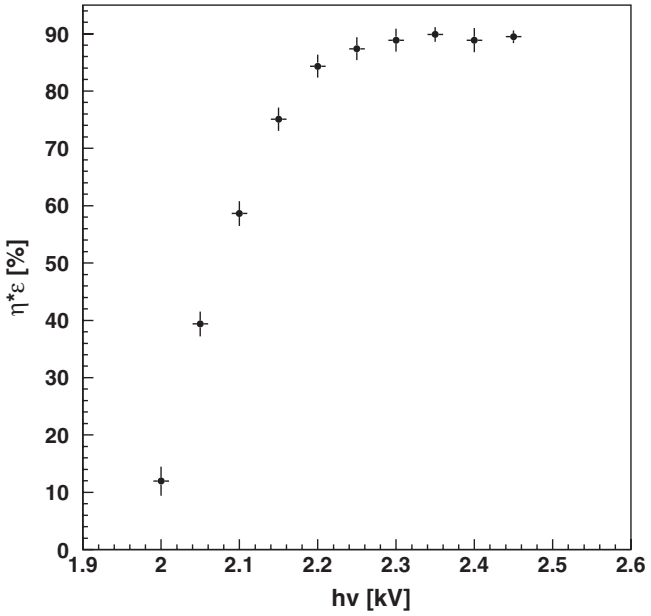

Fig. 25. Single tube track efficiency dependent on high voltage at a threshold voltage of 50 mV.

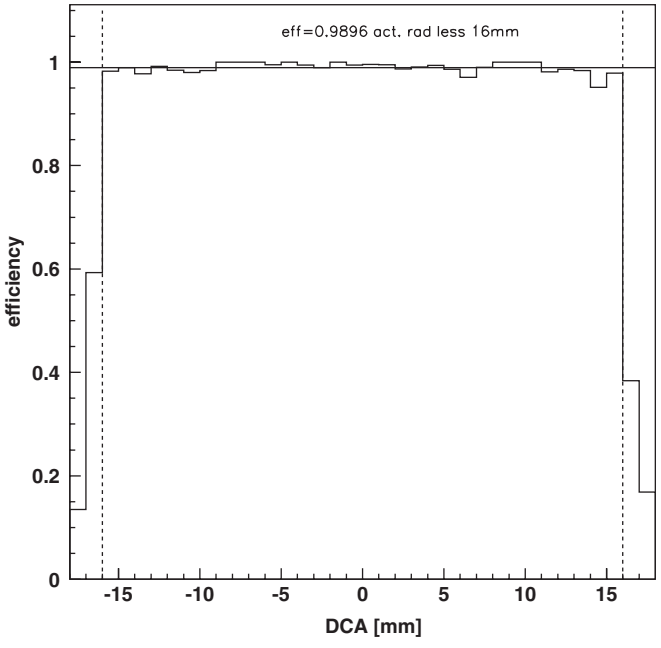

Fig. 24. Single tube hit efficiency versus the distance of the track to the wire.

distance of the track to the wire. An important drift tube parameter is the single tube track efficiency. It is defined as product of the single tube hit efficiency η and the probability ε that the hit gives the correct drift radius. The single tube track efficiency is shown in Fig. 25. At operating voltage the maximum of $\eta \times \varepsilon = 90\%$ has been reached.

8. Summary

In this paper we have described the design of the PT of the muon spectrometer of the OPERA detector. The challenge of the detector design originates from the tube length of 8 m, which has not been used before. An advantage of our design is the fact that no wire supports are necessary. Thus dead regions are avoided. The wire position accuracy of better than 150 μm is given by the endplates decoupled from the tube position accuracy. To minimize possibilities of gas leaks the gas connections between the tubes are located inside the endplates. The front end electronics was developed. The amplifier and discriminator are placed on the same board. Thus only digital signals are transmitted over long distances which reduces noise from the outside. The low cost electronics shows no oscillation behavior and does not need an additional shielding. Two small prototypes with 1 m tube length and one 8 m long prototype were successfully assembled in our mass production line. These modules were equipped with the electronic boards and operated in a cosmic setup. The bending of the vertical 8 m prototypes was measured to less than 300 μm. Adequate gas tightness was obtained. The signal attenuation over a tube length of 8 m is small enough to enable a safe operation. The spatial resolution was determinated to be better than 300 μm. Thus a momentum resolution of $\Delta p/p \leqslant 0.25$ can be achieved to guarantee a significant measurement of the muon sign. The single tube hit efficiency η was measured to better than 98%, the single tube track efficiency $\eta \times \varepsilon$ was measured to 90%. This results in a track efficiency of 97% for two PT planes.

Acknowledgements

We thank Yuri Gilitsky for assistance in the use of the L3 amplifier and Igor Tichomirov for the out-gassing measurements. Furthermore we thank the technical staff of our institute for the commitment and help to build the prototypes and tools. Special thanks to the DESY laboratory for the strong support concerning infrastructure and alignment of mass production tools and modules.

References

[1] M. Dracos, Phys. Atom. Nucl. 67 (2004) 1092.
[2] K. Kodama, et al., Nucl. Instr and Meth. 493 (2002) 45.
[3] S. Aoki, et al., Nucl. Instr and Meth. 488 (2002) 144.
[4] D. Duchesneau, Nucl. Phys. B 123 (Proc. Suppl.) (2003) 279.
[5] D. Autiero, Nucl. Phys. B 143 (Proc. Suppl.) (2005) 257.
[6] A. Airapetian, et al., ATLAS Muon Spectrometer Technical Design Report, CERN/LHCC/97-22, May 1997.
[7] F. Bauer, et al., Nucl. Instr and Meth. A478 (2002) 155.
[8] C. Ballhausen, R. Zimmermann, Test results of 8m drift tube prototypes for the high precision muon detector of OPERA, internal note, OPERA, August 2001.
[9] M. Calvetti, et al., Nucl. Instr and Meth. 174 (1980) 280.
[10] B. Koene, L. Linssen, Nucl. Instr and Meth. 190 (1981) 511.
[11] Y. Hoshi, M. Satoh, M. Higuchi, Nucl. Instr and Meth. A236 (1985) 82.
[12] Y. Asano, et al., Nucl. Instr and Meth. A254 (1987) 35.
[13] S. Bhadra, et al., Nucl. Instr and Meth. A269 (1988) 33.
[14] F.M. Newcomer, et al., Nucl. Instr and Meth. A283 (1989) 806.
[16] M. Capeans, Nucl. Instr and Meth. A515 (2003) 73.
[17] P. Rewiersma, The L3 Wire-Amplifier NH19-6112, NIKHEF-H, Amsterdam, February 1986.
[18] The L3 collaboration, The Forward Muon Detector of L3, Nucl. Instr. and Meth. A383 (1996) 342.
[19] data sheet MAXIM, www-maxim-ic.com, 2004.
[20] Multihit TDC V1190A/B, Technical Information Manual, CAEN, Reviews, vol. 3, 2004.
[21] H. van der Graaf, et al., Nucl. Instr and Meth. A419 (1998) 336.
[22] M. Cirilli, Nucl. Instr and Meth. A518 (2004) 62.
[23] M. Aleksa, W. Riegler, Non-Linear MDT Drift Gases like Ar/CO_2, ATLAS internal note, December 1998.
[24] A. Baroncelli, et al., Study of MDT Chambers Characteristics in Response to High Voltage and Discriminator Threshold Scan, ATLAS internal note, January 2000.
[25] R. Zimmermann, Zeitmesselektronik für den HERA-B-Detektor, Ph.D. Thesis, 1996 (German).